DTM-70-2

TECHNICAL SUMMARY REPORT

for

FABRICATION AND EVALUATION OF ALUMINUM HEAT PIPES

Contract No.: NAS5-11271

Goddard Space Flight Center

GSFC Technical Monitor: S. Ollendorf

Prepared by

Dynatherm Corporation
One Industry Lane
Cockeysville, Maryland

Program Manager: W. B. Bienert

for

Goddard Space Flight Center
Greenbelt, Maryland 20771

ABSTRACT

The objective of this program has been to evaluate the current heat pipe system on the OAO spacecraft and to increase its capability for future missions. A detailed analysis was made of the requirements, and approaches for the design of optimized heat pipes to meet future needs were identified. The experimental effort led to the development of a new, composite wick heat pipe which has significantly higher transport capability than those of current, conventional wick design.

FOREWORD

This technical report describes the work done under Contract NAS5-11271. The program was administered by the Goddard Space Flight Center, Greenbelt, Maryland. Mr. Stan Ollendorf was the NASA technical officer. Portions of the effort were monitored by Mr. Sam Willis of GSFC.

The work was completed by Dynatherm Corporation in Cockeysville, Maryland, under the direction of Dr. Walter Bienert. Mr. Patrick J. Brennan and Mr. Edward J. Kroliczek contributed to the experimental investigation.

TABLE OF CONTENTS

I. INTRODUCTION

The Orbiting Astronomical Laboratory (OAO) employs heat pipes for isothermalization of part of its structure. Three of the six levels of the spacecraft depend on circular heat pipes for equalizing the heat loads of their equipment bays. The heat pipes are being developed by Grumman Aircraft Corporation who is also the prime contractor for the spacecraft system.

Dynatherm Corporation has completed an evaluation of the OAO heat pipes and has developed alternate heat pipe configurations for future OAO missions. The program has confirmed the adequacy of the current heat pipe system. Advanced spacecraft may encounter heat loads, however, which are beyond the capability of conventional heat pipe technology. Part of the program, therefore, was aimed at developing heat pipes which will meet these future requirements. As a result, the composite wick concept has evolved which has a far higher heat transport capability than currently available heat pipes.

The program comprised the following tasks:

1. Evaluate the Heat Pipe Isothermalization System for OAO.
2. Design, fabricate, and test six (6) heat pipes of the type which are applicable to the OAO requirements.
3. Perform an analysis of the stability of operation of composite wick heat pipes.
4. Provide a theoretical model for the separation of working medium and non-condensing gas.

This report documents the work done under this contract during the period from January 8, 1970 through July 31, 1970. Following this introduction the results and

accomplishments of the program are reported. Technical details such as calculations are presented in the Appendices.

The organization of the report combines technically related subjects, rather than following the Statement of Work. However, reference to the Statement of Work is made frequently in order to verify compliance with its requirements.

II. RESULTS AND ACCOMPLISHMENTS

The work under this program can be logically divided into four (4) different categories:

A. Evaluation of the current OAO isothermalization system

B. Theoretical analysis of composite wick heat pipes, in particular those employing arteries

C. Development of a mathematical model for the interface between condensing and non-condensing vapors in a heat pipe

D. Development, fabrication and test of prototype heat pipes

In this section the results and accomplishments are presented, details of test and analysis are given in the appendices.

A. Evaluation of Current OAO Isothermalizer System

The OAO spacecraft is designed for one-year life in a 400-nautical mile earth orbit and is scheduled to be launched in 1970. The heat pipes are being flown primarily as an experiment to obtain design and integration experience and to isothermalize the spacecraft. Three heat pipes are incorporated in the B spacecraft and are mounted on its cylindrical structure. The pipes are made of 1/2-inch O.D. 6061 aluminum tubing and conform to the 48-inch I.D. spacecraft structure. A grooved wick structure was selected for these pipes. There are 30 longitudinal grooves, each approximately .030 inches wide and .035 inches deep. The working fluid is Freon 21. A detailed discussion of the OAO heat pipes is given in Reference II-1.

Ref. II-1: "Orbiting Astronomical Observatory Heat Pipes - Design, Analysis, and Testing," by Jonas A. Bilenas and William Harwell. ASME Paper No. 70-HT/SpT-9

Our evaluation of the OAO heat pipes consisted of a critical review of the applicable documents and an in-depth analysis of several key questions which could vitally affect their operation and/or have an influence on the temperature distribution of the spacecraft.

The analytical methods used for designing the OAO heat pipes and for evaluating the test results were found to be in agreement with current heat pipe technology (A-1)*. Particular questions such as the determination of dry-out conditions (A-3) and the possibility of blockage of a single saddle because of dry-out and/or overcharge (A-2) were adequately covered in the reviewed documents.

Our analysis therefore concentrated on the following specific problems:

1. Capillary pumping requirements in the presence of distributed heat sources and sinks

In Appendix A a "Heat Transport Parameter" is defined which is a useful tool for evaluating the capillary pumping requirement of a heat pipe with distributed heat sources and sinks. This parameter "Z" is defined as

$$Z = S_{max} - S_{min} \qquad \text{II-1}$$

where S_{max} and S_{min} are the extreme values of the function

$$S(x) = \int_0^x Q(x)\, dx \qquad \text{II-2}$$

The parameter Z has the dimension of "Watt-inches" and describes the capability of a heat pipe to transport a quantity of heat "Q" over a distance "L". It can be shown that "Z" is proportional to the maximum capillary pumping requirement.

* The numbers in parenthesis refer to specific paragraphs of the Statement of Work

In the case of a heat pipe which is characterized by an evaporator at one end and a condenser at the other and where the radial heat fluxes at evaporator and condenser are uniform the parameter "Z" becomes

$$Z = Q_{max}\left(\frac{1}{2} \quad L_E + L_A + \frac{1}{2} \quad L_C\right) \quad \text{II-3}$$

Q_{max} is the total heat transported and L_E, L_A, and L_C are the lengths of evaporator, adiabatic section and condenser, respectively.

In the case of a heat pipe with distributed loads "Z" must be evaluated using equations II-1 and II-2. This is done by computing the two extreme values of "S" from plotting the S (x) curve for the particular distribution of sources and sinks.

Typical load distributions for the # 4 spacecraft are given in GAC Memo PM-3/4-9-210 for levels 4, 5, and 6. A detailed analysis of the heat transport requirements of level 6 was made since it represents the highest load. The distribution of axial heat flow for this case is shown in Figure II-1, and the distribution of S (x) in Figure II-2. The maximum pumping requirement occurs between points A and B on the curve. The corresponding "Heat Transport Parameter" Z is

$$Z = S_{max} - S_{min} = 531.4 \text{ Btu-in/hr} = 44.2 \text{ Btu-ft/hr.}$$

This requirement is higher than the 34.11 Btu-ft/hr. computed by Grumman. The approach used by Grumman was to calculate the area under each segment a through d of the Q, versus x curve, and then to select the largest of these areas as the maximum $\int Q dx$. This method is wrong and leads to an underestimation of the heat transport requirements. It implies that each of the sections

FIGURE II-1

DISTRIBUTION OF AXIAL HEAT FLOW

OAO HEAT PIPE, LEVEL 6, #4 SPACECRAFT

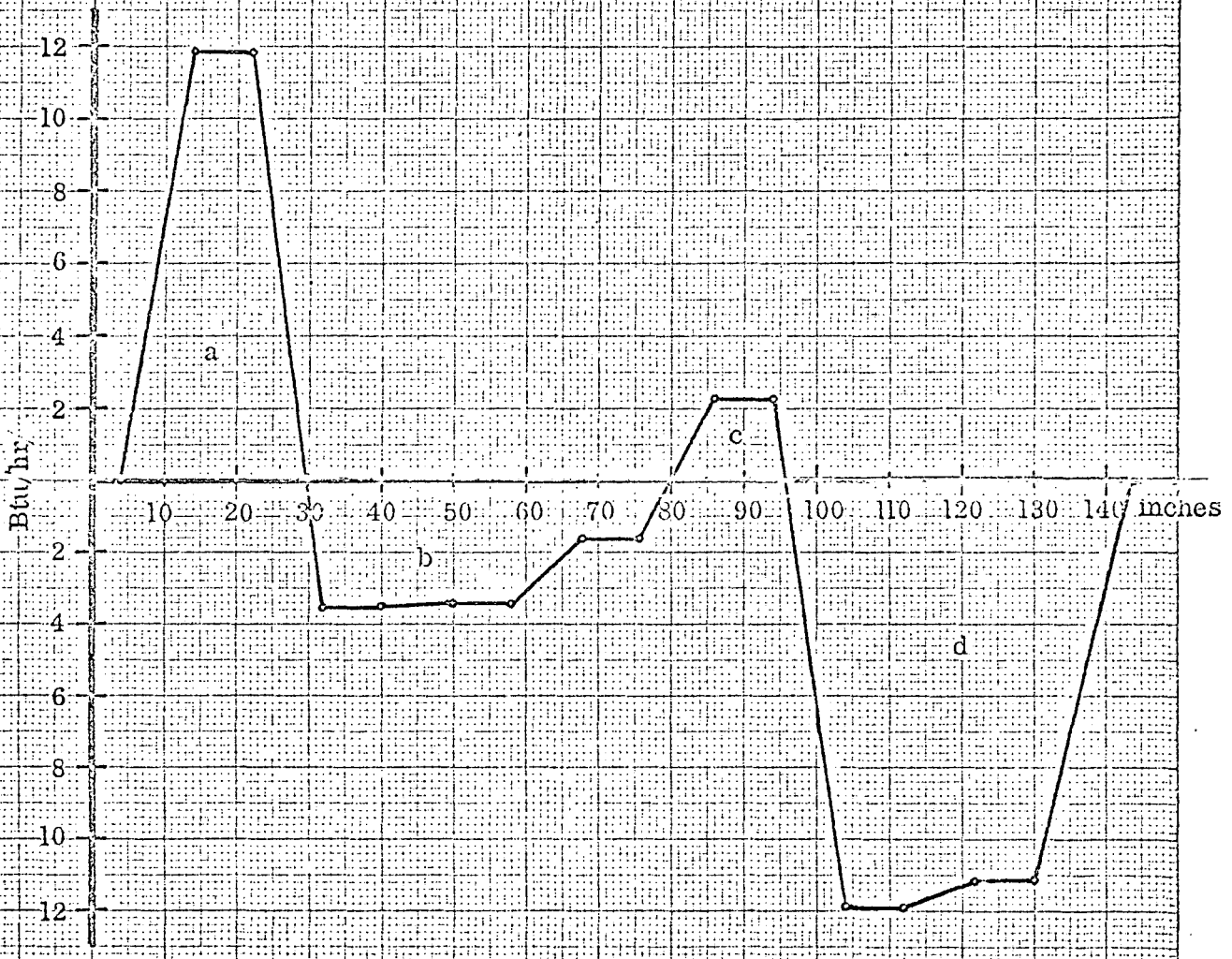

FIGURE II-2

HEAT TRANSPORT PARAMETER S(x)

OAO HEAT PIPE, LEVEL 6, #4 SPACECRAFT

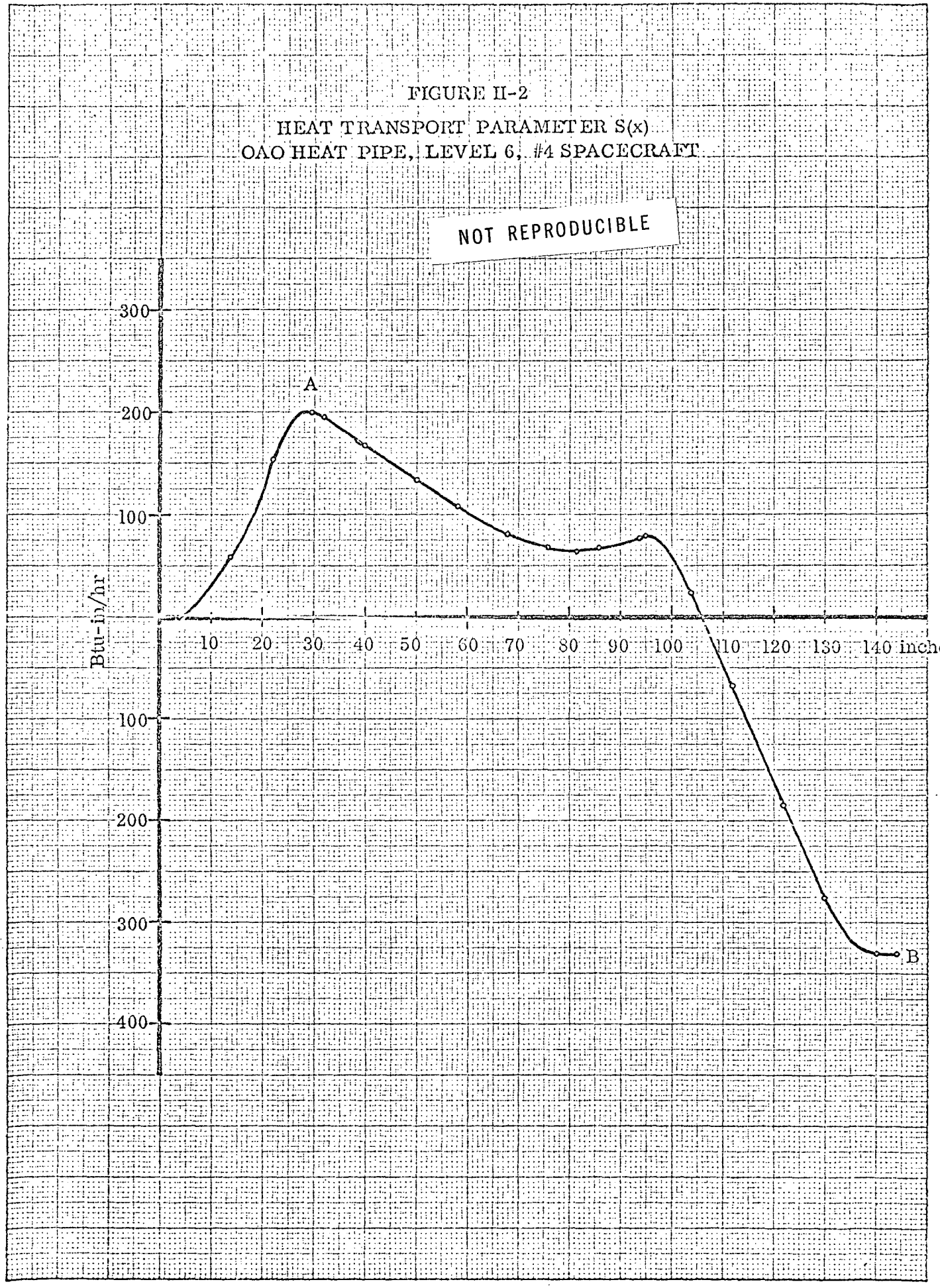

a, b, c, and d is independent of each other and has its own pressure distribution. In reality the heat pipe is one single vapor chamber. The pressure in the liquid can never exceed that of the vapor. At one point (A) the liquid pressure is equal to that of the vapor, corresponding to an infinite radius of curvature of the meniscus. The lowest liquid pressure exists at point B, where the meniscus has the smallest radius of curvature and maximum capillary pumping occurs. The maximum heat transport requirement exists between these two extreme points and the heat pipe must be designed to handle these requirements.

2. Capillary Pumping of Grooves in a Gravity Field

In zero gravity, each individual groove of a grooved heat pipe contributes equally to the heat transport capability. In a gravity field, however, the pumping capability of the upper grooves is somewhat reduced. As shown in Appendix D, a groove which is inclined by an angle α with respect to the vertical has a capillary pumping capability equal to

$$\Delta P_{Cap} = \frac{2\sigma}{w} - \rho g d \cos\alpha \qquad \text{II-4}$$

(σ is the surface tension of the liquid, w and d are the width and depth of the groove, respectively, ρ the liquid density, and g the gravitational constant).

The first term in equation II-4 represents the pumping without gravity, the second one the reduction in a gravity field. The performance of the entire heat pipe must be evaluated by analyzing each groove separately and then adding the contributions of all grooves.

A grooved heat pipe has an important advantage over those with other capillary structures. The liquid in one groove does not communicate with the liquid in the others. Consequently, when considering the influence of gravity, each groove may be treated separately. In other words, the characteristic height which determines the static head in a gravity field is not the tube diameter but the depth of the groove. There is some experimental evidence* that the liquid from the upper grooves in the OAO pipe has a tendency to drain. This is a characteristic of the current groove design which permits some "leakage," probably near the ends of the pipe. Attention should be paid to this effect in future groove designs because its elimination would enhance the capillary pumping capability.

3. Nucleate Boiling Within Grooves (A-4)

A model for the heat transfer in the evaporator of a grooved heat pipe has recently been published. (Ref. II-2) Because of the large difference in the thermal conductivity between the fin and the liquid essentially all the heat is conducted along the fins and from the fin-tip to the surface of the liquid.

At the bottom of the groove the liquid is slightly superheated, the amount of superheat being determined by the ΔT through the fin. This superheat is accompanied by an increased vapor pressure which could lead to nucleate boiling. Nucleate boiling is synonymous with the formation of vapor bubbles. It is harmless if the bubbles collapse immediately after formation, but it leads

---

* Private communication by W. Harwell of Grumman Aircraft Corporation

Ref. II-2 "Optimum Cryogenic Heat Pipe Design" by Patrick Joy, RCA, Camden, N. J. ASME Paper No. 70-HT/SPT-7

to vapor blockage and dry-out of the grooves if the bubbles persist. The criterion for bubbles to collapse is that the vapor pressure inside the bubble (which is determined by the amount of superheat) is less than the capillary pressure of the bubble, i.e.

$$\Delta P_{Superheat} \leq \frac{2\sigma}{r} \qquad \text{II-5}$$

According to II-5 small bubbles will always collapse. If the bubble size exceeds a certain radius r_c the bubbles will no longer collapse but will grow. In a groove, the maximum bubble radius is equal to w/2, where w is the width of the groove. If the superheat is such that bubbles will collapse even if they reach their maximum possible size, then dry-out and existence of stable vapor bubbles is impossible. The maximum permissible superheat is thus given by

$$(\Delta P_{Superheat})_{Max} = \frac{2\sigma}{w/2} \qquad \text{II-6}$$

The superheat is related to the heat flux through the conduction along the fin and the Clausius-Clapeyron relation.

For the OAO heat pipes the maximum heat input per saddle is 11.88 Btu/hr (Level 6 Saddle F OAO-C), and the corresponding superheat at the bottom of a groove is $2.0 \times 10^{-2}{}^{\circ}F$. The superheat which will lead to a stable bubble with a diameter equal to the width of the groove is calculated to be $2.9 \times 10^{-2}{}^{\circ}F$. Thus the actual heat fluxes experienced on the OAO spacecraft

will not lead to nucleate boiling. It should be pointed out, however, that the above model is extremely conservative. Tests with many heat pipes have shown that much higher heat fluxes can be applied before nucleate boiling occurs.

B. Theoretical Analysis of Composite Wicks (A-5) (A-7)

Composite wicks have a high theoretical heat transport capability. Typically, they consist of structures in which the capillary pores are optimized independently of the dimensions of the liquid flow channels. In a conventional wick, such as a homogeneous wire mesh, the pores serve a dual function: they provide the capillary pumping and are the flow passages with the accompanying viscous pressure drop. In a typical composite wick, such as an artery, the capillary pumping is provided by the openings of the screen forming the artery while the artery itself constitutes the flow passage. Here, in contrast to the conventional wick, the diameter of the flow channels may exceed the capillary pore size by orders of magnitude.

An example of the potential of composite wicks is shown in Figure II-3 for the case of an arterial wick. The lower curve gives the maximum heat transport capability of a single artery as a function of its diameter. The artery is assumed to be not quite filled; i.e., the pumping is done by the artery itself and it acts like a conventional wick. The upper curve shows the heat transport capability of the same artery, but now the artery is completely filled and the 200 mesh screen forming the artery is responsible for the capillary pumping.

Although they have high theoretical heat transport capability composite wicks are difficult to use in practical heat pipes. The full pumping capacity is only available

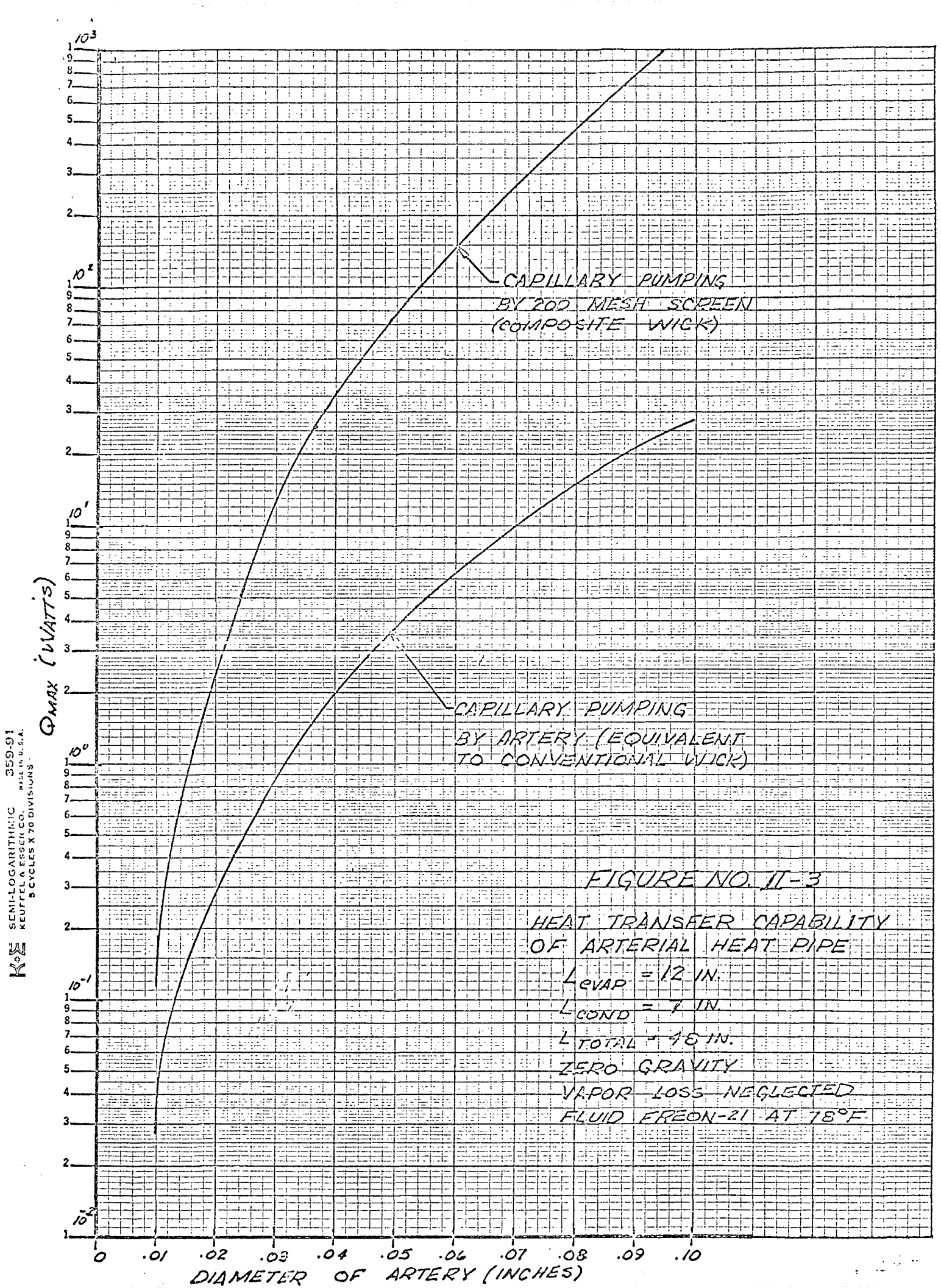

FIGURE NO. II-3

HEAT TRANSFER CAPABILITY OF ARTERIAL HEAT PIPE

L_{EVAP} = 12 IN.

L_{COND} = 7 IN.

L_{TOTAL} = 48 IN.

ZERO GRAVITY

VAPOR LOSS NEGLECTED

FLUID FREON-21 AT 78°F

when the wick is completely filled. In intermediate situations (partial fill) the capillary miniscus is determined by the dimensions of the flow channel resulting in greatly reduced performance. Partial fill of the composite wick could be the result of:

a. Incomplete filling during startup

b. Formation of bubbles during operation because of excessive heat load

c. Formation of bubbles and draining due to shock and vibration

A detailed investigation of the start-up (priming) and stability problems associated with composite wicks was completed. Several glass heat pipes containing various artery designs were built and used for studying the phenomena.

During initial charging of the heat pipe the liquid gradually wets the entire wick. In the case of an arterial wick the tendency prevails for the liquid to at first wet the walls of the artery before the interior of the artery is filled. Any vapor or gas trapped within the artery has no way to escape once the liquid membrane surrounding the artery has been formed. As a result, bubbles occur within the artery which may range in size from less than one artery diameter to long "sausage" like bubbles which extend over long sections of the heat pipe. The bubbles were found to be very stable, although eventually they do almost always collapse. The rate of the collapsing of a typical elongated bubble was measured to be in the range of 10^{-4} cm/sec.

Bubbles of the kind described are not only generated during initial filling of the heat pipe but every time the artery is drained and refilling is attempted.

The existence of bubbles prevents the artery (or any other composite wick) from properly operating. This may be explained as follows: At maximum heat load the

capillary pumping is determined by the pore size of the screen forming the artery. If a bubble exists within the artery the radius of the bubble controls the pumping.* In the extreme case of a bubble filling an entire section of the artery the pumping capability is reduced to that of an open artery.

In order to realize the full capability of an arterial wick bubbles must be avoided at any rate. One method to avoid bubbles is to prevent their formation in the first place. The use of an open ended artery or its construction of a single layer of screen are possible techniques. The other method is to assure that bubbles will rapidly collapse once they have formed.

The described techniques for avoiding the formation of bubbles have been demonstrated experimentally. The open ended artery can be filled free of bubbles by letting the gas or vapor escape through the open end. The benefit of an artery made from a single layer of screen has been shown in laboratory experiments with a glass heat pipe.

The mechanism under which bubbles collapse rapidly once they have been formed requires an investigation of their stability. This analysis has been performed and the details are presented in Appendix C. The results are as follows:

1. In the absence of temperature gradients and non-condensible gas all bubbles will collapse. The rate of collapse is of the order of fractions of a second.

2. Temperature gradients of the order of .01^{o}K can create stable bubbles. Fluids with high vapor pressure are much more sensitive to temperature

*The radius of a stable bubble is always larger than the pore size, otherwise it would escape.

gradients than those with low vapor pressure. However, a temperature gradient can hardly explain the observed slow collapse of the bubbles. Temperatures should equalize much faster and should result in more random growth and collapse of bubbles.

3. The presence of non-condensing gases are the only plausible explanation for the observed stability of bubbles. The slow collapse is due to the gradual dissolving of the gas in the liquid. Only very small amounts of non-condensing gas are required to create relatively stable bubbles. As an example, with methanol as a working fluid, a partial pressure of non-condensing gas of less than 1 Torr suffices to create stable bubbles.

Based on this analysis it was concluded that composite wicks can be employed successfully if either non-condensing gases are completely eliminated or if proper means for venting the artery are found. Construction of the artery from a single layer of screen (which prevents the formation of a liquid membrane) appears to be the most practical approach at the present time. A single layer of screen is not self-wetting. Therefore, the liquid membrane which can trap gas bubbles within the artery does not easily form. During filling of the artery the gas can escape until the filling is complete. If a gas bubble is generated during operation the liquid membrane will normally persist and thus prevent the artery from refilling. However, the membrane can easily be destroyed by locally over heating a section of the artery and refilling occurs spontaneously. This technique has been demonstrated repeatedly in the laboratory.

C. Mathematical Model of Gas Interface (A-6)

In a heat pipe containing a non-condensing gas in addition to the working fluid, separation of the two media occurs. An analysis has been conducted to examine the

profile of the interface, i.e., the distribution of concentration and temperature along the pipe. The problem may be expressed analytically by a set of twelve (12) equations along with the applicable boundary conditions. The derivation of the equations is given in Appendix D. Numerical solutions could easily be obtained with standard computer routines. Such results would contribute greatly to the understanding of the behavior of variable conductance heat pipes.

D. Development, Fabrication and Test of Prototype Heat Pipes

Six aluminum heat pipes were fabricated, tested and delivered. A summary of the heat pipe designs is given in Table II-1 and the test set-up is described in Appendix E. The first four pipes (Serial No. -1, -2, -4, and -5) represent heat pipes with conventional wicks, the last two (Serial No. -6 and -7A) have composite wicks. Results of performance checks are given in Figures II-4, II-5, and II-6.

The pipe with plain grooves as a wick performed best among the three Freon heat pipes. Heat pipe No. -2 was expected to give a much higher heat transport capability since the screen covered grooves should function as a composite wick. The fact that the addition of the screen did not enhance the heat transport capability indicates that capillary pumping due to the screen was not present. The slight reduction of the performance compared to the plain grooved pipe was attributed to a draining of the upper grooves. By adding the screen, all grooves are referenced to the bottom of the pipe. In the case of a fluid with low surface tension, such as Freon 21, the upper grooves will not be able to maintain the capillary head of the 1/2" diameter tube and will dry out.

Heat pipe No. -5 has a considerable higher heat transport capability than the

Table II-1

Summary of Aluminum Heat Pipes

Heat Pipe Serial No.	Fluid	Charge	Wick Structure	Remarks
S.O. 0019-1	Freon 21	35.03 g	Plain grooves (Tubing GFE)	
S.O. 0019-2	Freon 21	39.10 g	Grooves covered with 200 mesh SS screen (Tubing GFE)	
S.O. 0019-4	Freon 21	40.80 g	20 Mil annulus formed by 200 mesh screen	
S.O. 0019-5	NH_3	6.27 g	Plain grooves (Tubing GFE)	20" long pipe
S.O. 0019-6	CH_3 OH	19.28 g	Artery (.090" dia) formed from 200 mesh SS screen. Bridges connecting artery with wall formed from 2 layers of 200 mesh SS screen. Circumferential grooves in wall (.005 deep, 48 grooves per inch)	Artery open on one end
S.O. 0019-7A	CH_3 OH	17.55 g	Artery (.062" dia), otherwise identical to No. 6.	Artery closed on both ends.

FIGURE II-4

RESULTS OF PERFORMANCE CHECK

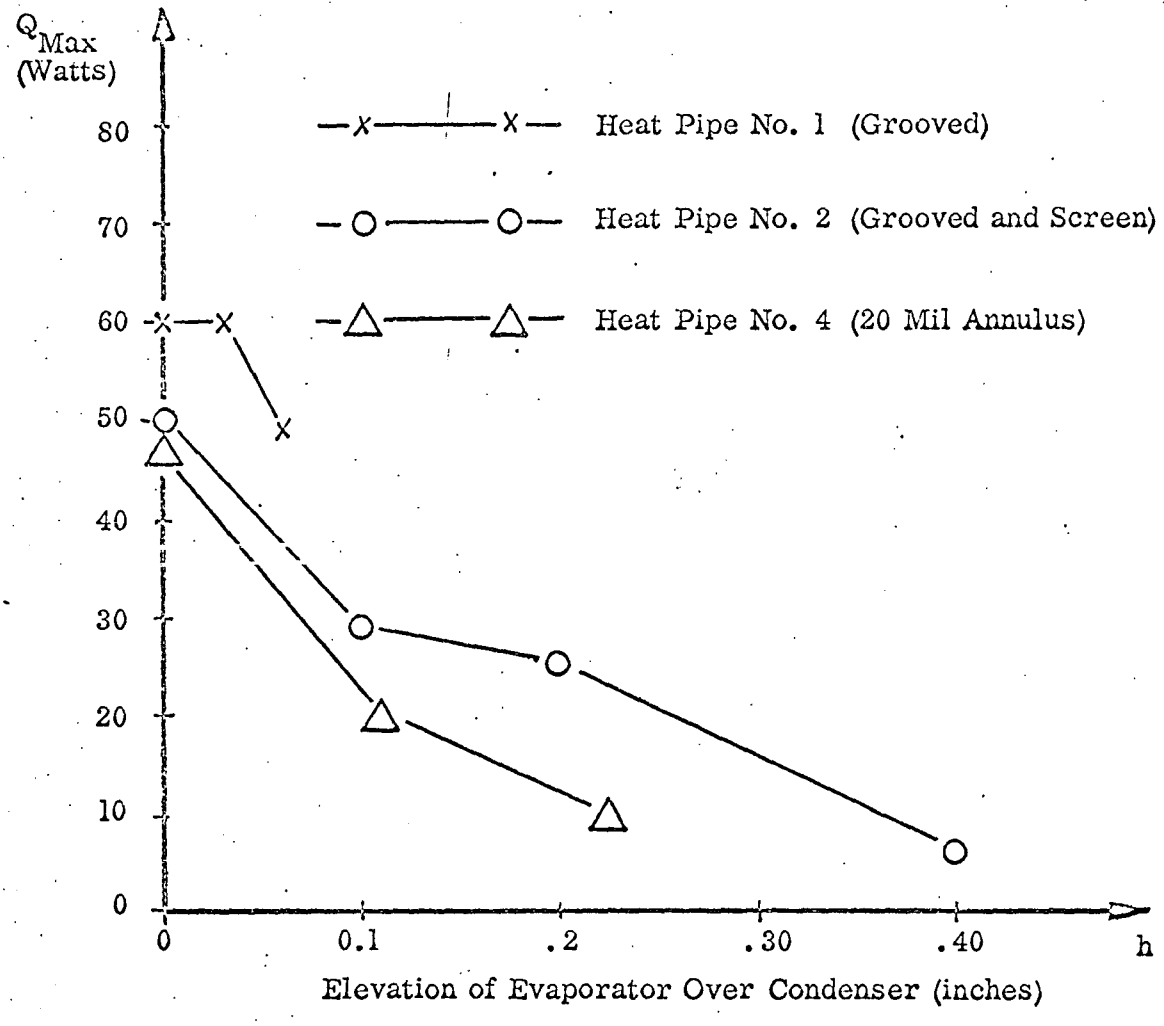

FIGURE II-5

RESULTS OF PERFORMANCE CHECK

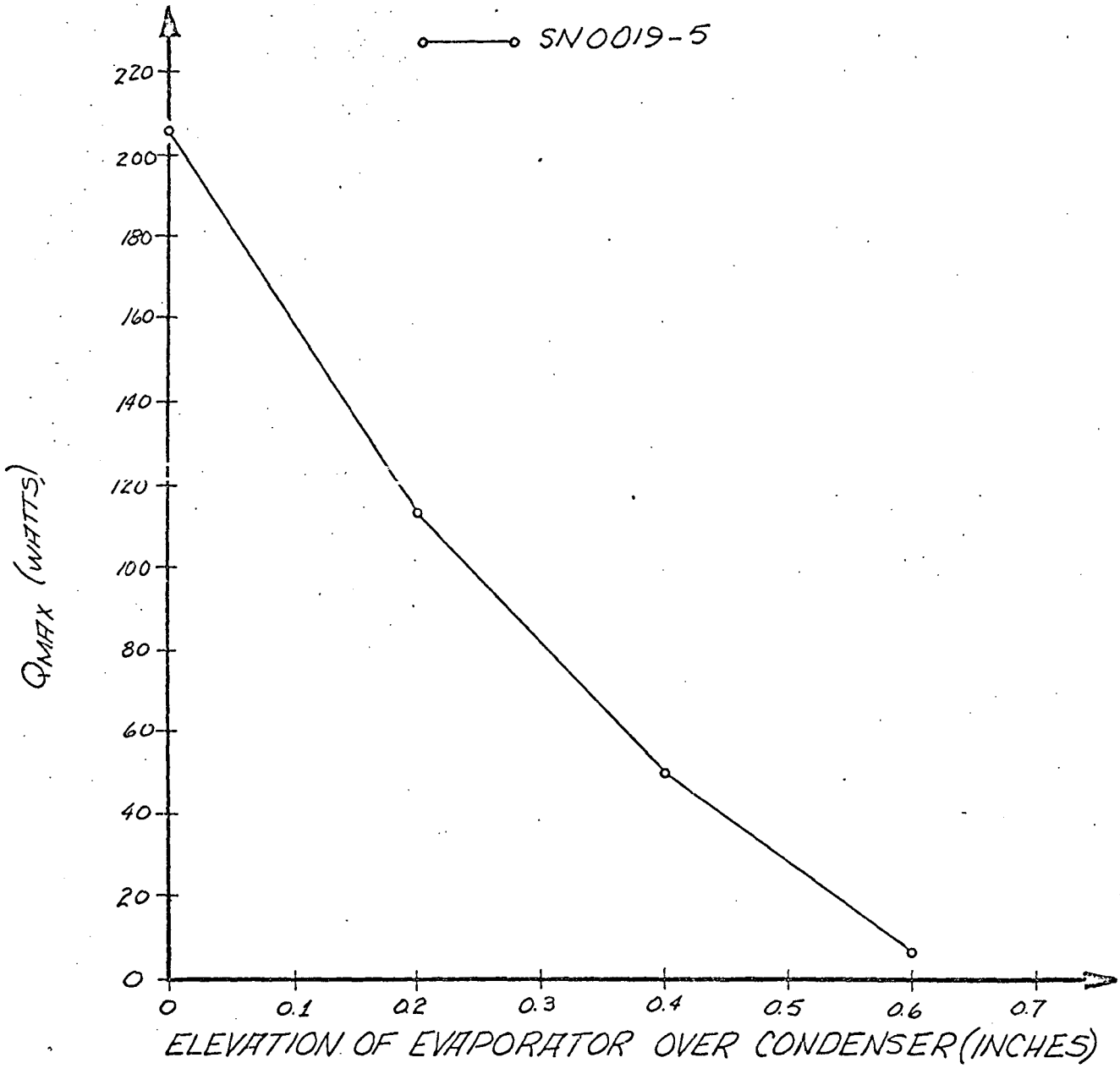

FIGURE II-6

RESULTS OF PERFORMANCE CHECK

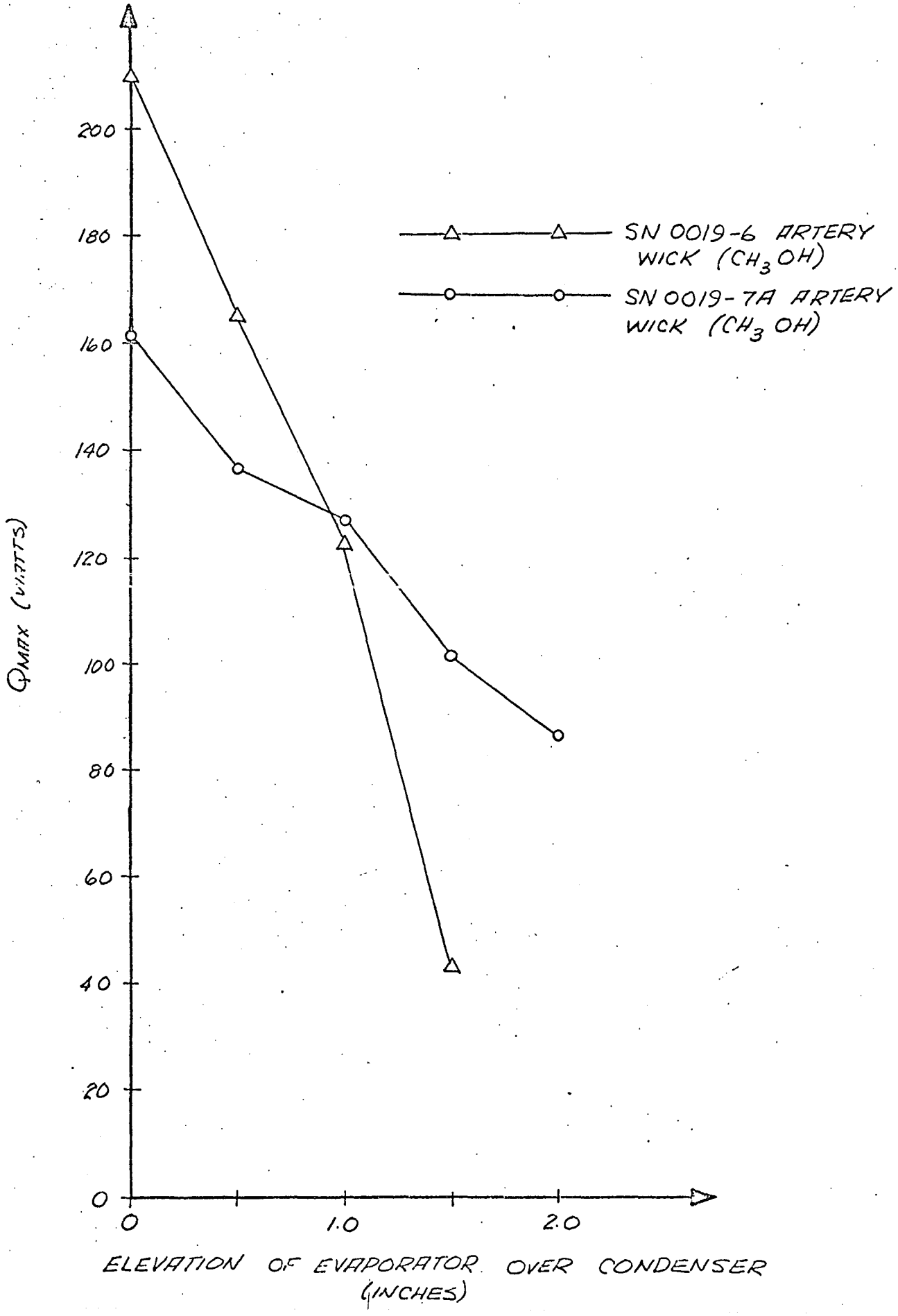

three Freon pipes. This improvement is due to the shorter transport length and to the different working fluid. Ammonia has a higher liquid transport factor than Freon 21. However, the measured improvement is not consistent with the better fluid properties. The measured "Heat Transport Parameter" Z for pipe No. -5 was only 2800 w-inches compared to 2250 w-inches for pipe No. -1. By comparison, the liquid transport factor of NH_3 is more than twice that of Freon 21. This discrepancy will be further investigated by refilling heat pipe No. -1 with NH_3 and comparing the two fluids within the same pipe.

The two methanol heat pipes (No. -6 and -7A) have arterial wicks which are representative of composite wicks. Methanol was chosen as the working fluid on the basis of preliminary experiments with five different fluids:

Freon 21

Ammonia

Methanol

Acetone

Dow therm-E

The first two fluids have a relatively high vapor pressure at room temperature, and it was difficult to fill the artery. The last three fluids have low vapor pressures and filling was readily achieved. Methanol was selected because it has the highest liquid transport factor among the three low pressure fluids. Heat pipe No. -6 was a .090" diameter artery which is open at the condenser end. Filling of the artery is achieved by lowering the evaporator end thus letting any gas bubbles escape through the open end of the artery. Heat pipe No. -7A has a .062" diameter artery which is closed

on both ends. The smaller artery diameter was chosen in order to facilitate self-filling in a gravity field. This pipe was tested in a horizontal orientation as well as with the evaporator elevated. The artery filled itself consistently without tilting the pipe from the horizontal.

The heat transport capability of the two pipes with composite wicks is significantly higher than those with conventional wicks. The improvement becomes particularly evident when operating the heat pipe with the evaporator elevated. The theoretical potential of the arterial heat pipes is even higher than currently achieved in the laboratory. Additional development effort is therefore desirable to realize the full potential.

APPENDIX A

HEAT TRANSPORT PARAMETER OF A HEAT PIPE

This Appendix defines and discusses a "Heat Transport Parameter" which is a useful measure of the capability of any given heat pipe. This parameter "Z" has the dimension "Watt-inches" and describes the capability of a heat pipe to transport a quantity of heat "Q" over a distance "L".

Consider a tubular heat pipe with a given distribution of heat sources and heat sinks along its length. The axial heat flow "Q (x)" will, in general, vary along the pipe. In the laminar flow regime the viscous pressure loss per unit length will be proportional to the heat flow. Hence, the pressure difference between any two points A and B of the heat pipe will be given by

$$(\Delta P_{Viscous})_{A-B} = C \int_{A}^{B} Q(x)\, dx \qquad \text{A-1}$$

The proportionality constant "C" is determined by the geometry of pipe and wick and by the properties of the working fluid. An expression for C is derived, for example, in Reference A-1 for the case where the viscous pressure loss in the liquid is dominating.

In a heat pipe, the pressure losses in the liquid are balanced by capillary pumping. The capillary pumping requirement between any two points, A and B, is therefore also given by equation A-1. In order to design a heat pipe for a specified heat load the maximum pumping requirement must be known. According to equation A-1 the maximum pumping requirement is determined by selecting the two end points, A and B, of the integration such that the integral reaches its highest possible value.

Ref. A-1: "Heat Pipe Design Manual", MND-3288, Martin-Marietta Nuclear Division, February 1967

For the purpose of evaluating the maximum pumping requirement the following auxiliary parameter "S" is defined:

$$S(x) = \int_0^x Q(x)\,dx \qquad \text{A-2}$$

The integration is carried out from one end of the heat pipe (x = 0). The variation of S along the heat pipe is proportional to the changes of pressure within the liquid phase of the working fluid.

We are now in the position to define the "Heat Transport Parameter" as follows:

$$Z = S_{Max} - S_{Min} \qquad \text{A-3}$$

Z is evaluated by selecting the maximum and minimum values of the S (x) distribution. The technique of computing Z will be demonstrated shortly in two representative examples.

The correlation between Z and the required capillary pumping follows from equation A-1:

$$\Delta P_{Cap} = C\,Z \qquad \text{A-4}$$

The Heat Transport Parameter Z is a useful tool for thermal modeling of a heat pipe. Z determines the transport requirements uniquely. Once its value has been computed, the capillary pumping ΔP_{Cap} and the geometry of wick and pipe can be selected. Conversely, for a given heat pipe the invariance of Z can be met by various lengths and distribution of heat loads.

Two typical examples follow:

a. Heat Pipe With Evaporator and Condenser at Extreme Ends

The radial heat distribution for this example is shown in Figure A-1. Heat is uniformly applied over the length (L_e) of the evaporator and rejected uniformly over the length (L_c) of the condenser. Part of the heat pipe (L_a) comprises an adiabatic section with no radial heat transfer. The axial

FIGURE A-1

HEAT FLOW DISTRIBUTION IN A HEAT PIPE WITH EVAPORATOR AND CONDENSER AT EXTREME ENDS

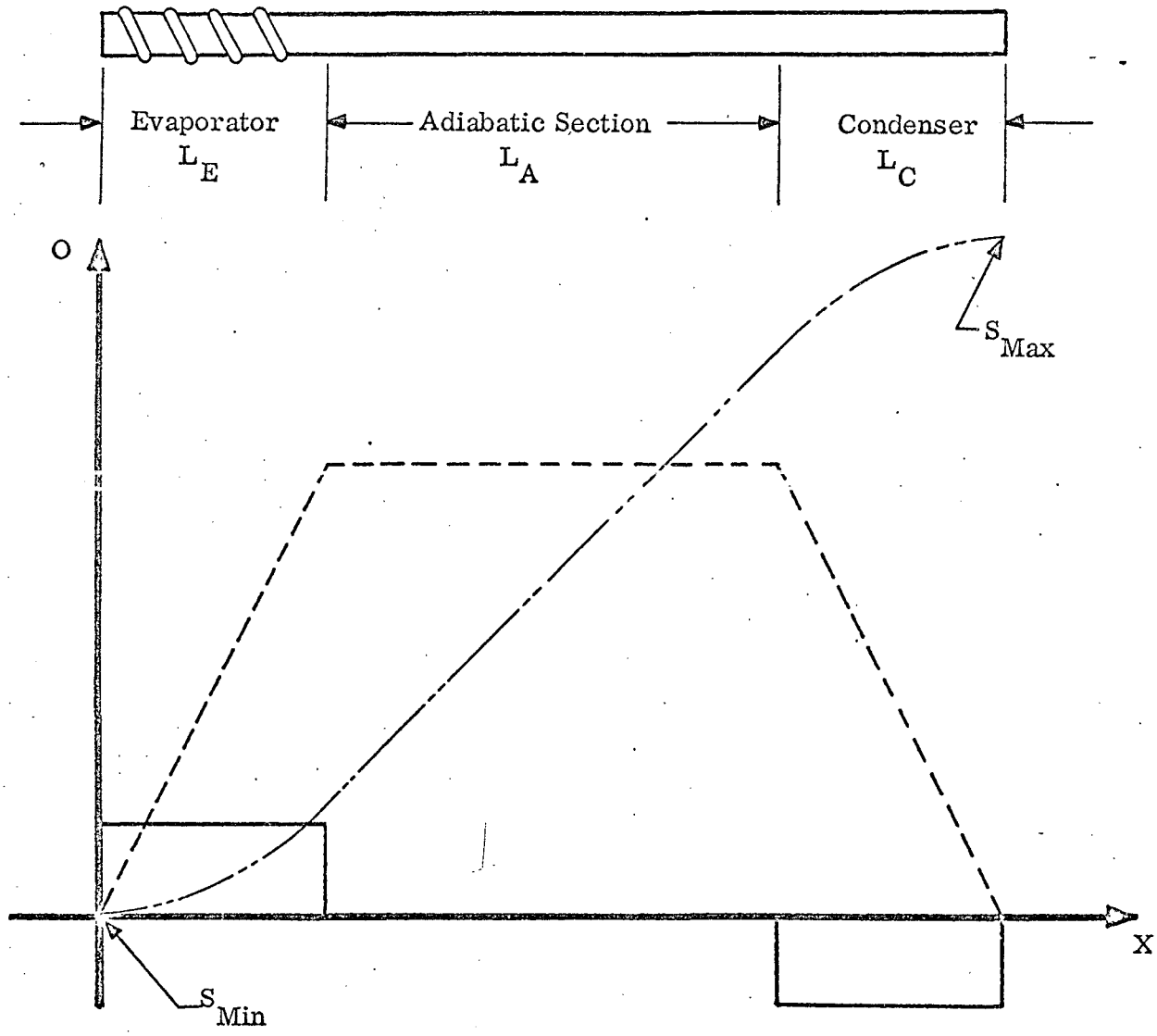

——— Radial Heat Flow at Evaporator and Condenser

– – – – – Axial Heat Flow

—·· ——— Parameter $S = \int_0^x Q\,dx$

heat flow Q (x) is also shown in Figure A-1. It is obtained by integrating the radial heat flows along the length of the pipe, viz

$$Q(x) = \int_0^x q_r \, dx \qquad \text{A-5}$$

The axial heat flow increases at first linearly along the evaporator, then remains constant at the adiabatic section, and finally decreases linearly to zero at the condenser.

From equation A-2 it follows that S (x) rises at first parabolically, then linearly and again parabolically at the condenser. The maximum and minimum values of S occur at the two ends of the heat pipe. Hence, the maximum capillary pressure difference also occurs between these two extreme points. According to equations A-2, 3, and 4 the capillary pumping requirement is given by

$$P_{Cap} = C \int_O^L Q(x) \, dx \qquad \text{A-6}$$

i.e., by extending the integration from one end of the heat pipe to the other.

For the present example the parameter Z may be expressed in terms of an effective flow length L_{Eff}. It is defined by the equation

$$Q_{Max} \cdot L_{Eff} = \int_O^L Q \, dx \qquad \text{A-7}$$

It can easily be shown that L_{Eff} is related to the geometry of the sample heat pipe through

$$L_{Eff} = \frac{1}{2} L_E + L_A + \frac{1}{2} L_C \qquad \text{A-8}$$

This simple relationship between L_{Eff} and the length of various heat pipe sections holds only if the radial heat fluxes at evaporator and condenser

are uniform

b. Heat Pipe With Distributed Heat Input and Output Zones

In this example (Figure A-2) several evaporator and condenser zones are distributed along the length of the heat pipe. (The radial heat flux within each zone does not necessarily have to be uniform.) The axial heat flux is obtained from equation A-5. In the most general case Q will vary along the length of the pipe and may even change direction. By integrating Q along the pipe the parameter S is obtained as a function of axial position x. In this example S no longer rises monotonously but may have several maxima and minima. The capillary pumping requirement is again defined by equation A-4, viz:

$$P_{Cap} = C Z = C (S_{Max} - S_{Min}) \qquad A-9$$

However, in the present example the pumping requirement can no longer be calculated by integrating between the two end points of the heat pipe (equation A-6). The proper procedure is to select the difference between two extreme values S_{Max} and S_{Min}. In the example given in Figure A-2 the value of the integral between the two end points is actually zero although the Heat Transport Parameter "Z" is definitely finite.

FIGURE A-2

HEAT FLOW DISTRIBUTION IN A HEAT PIPE WITH DISTRIBUTED HEAT INPUT AND OUTPUT ZONES

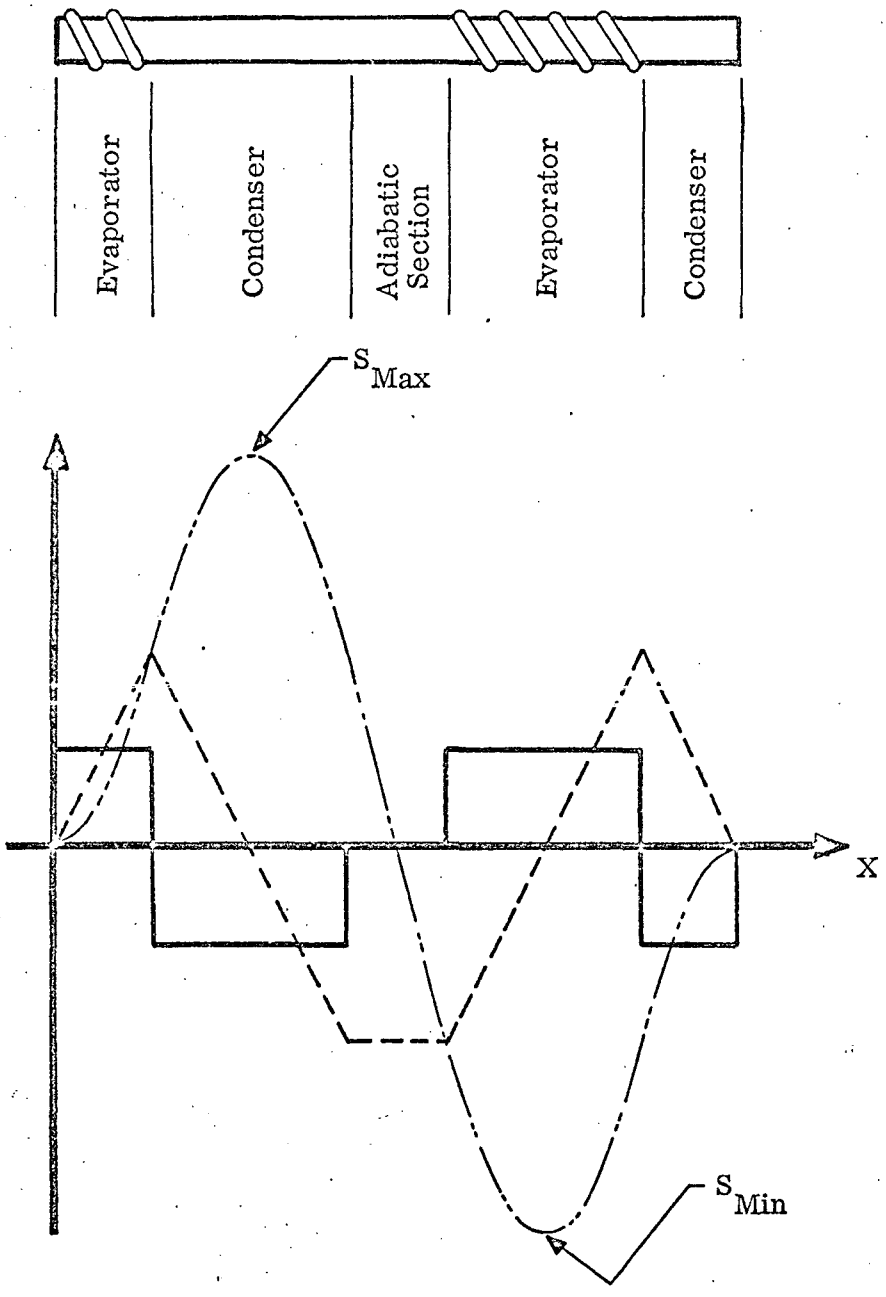

——— Radial Heat Flow at Evaporator and Condensers

– – – – – Axial Heat Flow

——– – ——– Parameter $S = \int_0^x Q\,dx$

APPENDIX B

CAPILLARY PUMPING OF GROOVES IN A GRAVITY FIELD

This discussion deals with the capillary pumping in a grooved heat pipe which is oriented horizontally. Typically, the grooves are evenly spaced, are an integral part of the tube wall, and separated from each other by "lands." Figure B-1 shows the groove geometry of the OAO heat heat pipes.

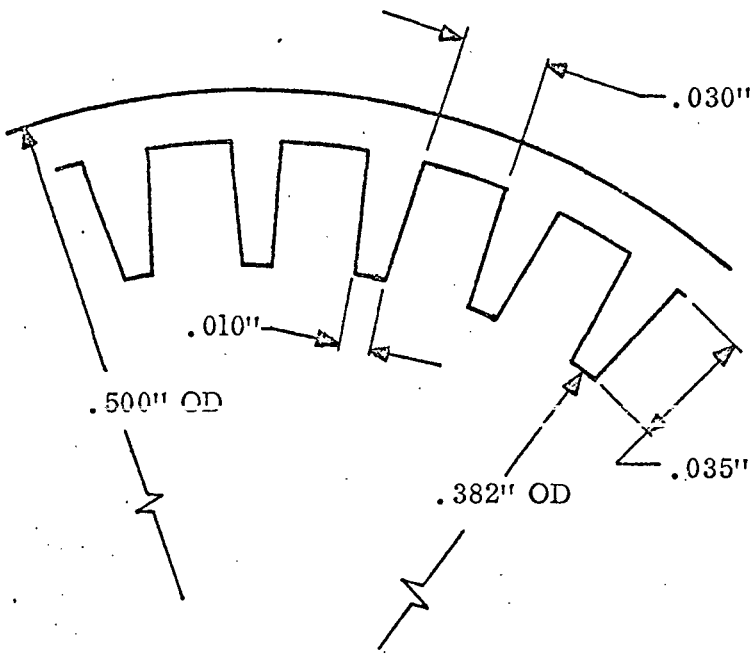

FIGURE B-1
GROOVE GEOMETRY OF OAO HEAT PIPES

First we observe that each groove represents an individual capillary. The liquid in one groove does not communicate with the liquid in the next one. Consequently, the pressure of the liquid in each groove is independent and is not related to any reference such as a pool at the bottom of the heat pipe. When considering the influence of gravity each groove may be treated separately. By contrast, in a conventional screen type wick structure, the pressure within the liquid at the top of the pipe is related to

the pressure at the bottom by the following equation

$$p_{Top} = P_{Bot} - \rho g D \qquad \text{B-1}$$

where D is the tube diameter. In many heat pipes, the static head associated with its diameter is comparable to the capillary pumping capability and, as a result, the upper portions of the wick contribute to the heat transport only in a greatly reduced manner. To say it differently, most of the available capillary pumping is used up to hold the liquid in the wick and is not available for liquid transport.

A grooved heat pipe is not subject to this limitation. The individual grooves communicate with each other only by condensation and evaporation, i.e., through the vapor. Because of the low vapor density, the static head corresponding to one tube diameter is negligible.

Having established that each groove acts as an individual capillary, we will now proceed to examine the effect of gravity on the capillary pumping. Consider the single groove shown in Figure B-2. Its orientation with respect to gravity is defined by the angle α, its width is w and its depth d.

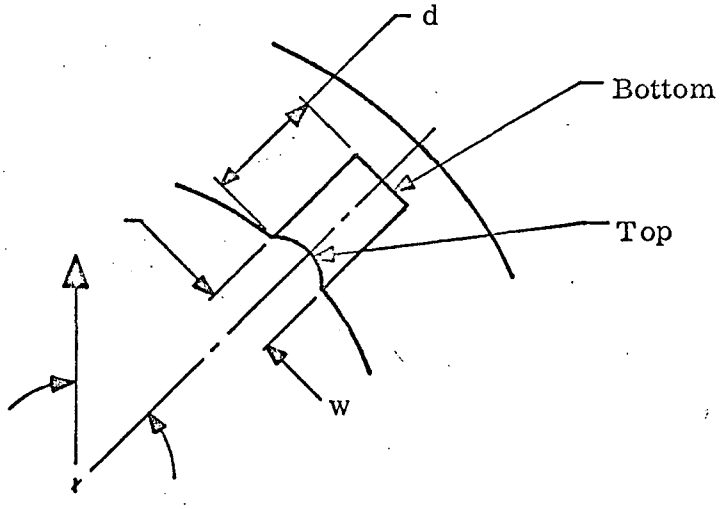

FIGURE B-2

EFFECT OF GRAVITY ON SINGLE GROOVE

The liquid-vapor interface will have a miniscus with a radius r which is defined by the inequality

$$\frac{w}{2} < r < \infty \qquad \text{B-2}$$

Since the liquid is assumed to be in equilibrium with its vapor the hydrostatic pressure in the liquid may be written as

$$p_l = p_v - \frac{\sigma}{r} \qquad \text{(at bottom of groove)} \qquad \text{B-3}$$

$$p_l = p_v - \frac{\sigma}{r} + \rho\, g\, d \cos \qquad \text{(at top of groove)} \qquad \text{B-4}$$

σ is the surface tension of the liquid, ρ its density and p_v the equilibrium vapor pressure. The liquid is held in the groove by a balance of pressures across the interface between liquid and vapor, i.e., it is held if

$$p_v \geq p_l = p_v - \frac{\sigma}{r} + \rho\, g\, d \cos \qquad \text{B-5}$$

(The term p_v on the left side of B-5 represents the pressure of the vapor phase of the working fluid which, by definition, is equal to the equilibrium vapor pressure). Equilibrium B-5 can be rewritten to yield

$$\frac{\sigma}{r} \geq \rho\, g\, d \cos \alpha \qquad \text{B-6}$$

The last equation defines the maximum radius of curvature which the miniscus may have while still supporting the liquid.

The capillary pumping is determined by the maximum difference of the hydrostatic pressure between condenser and evaporator. The average liquid pressure in a groove at the condenser is

$$\overline{p_c} = p_v - \frac{\sigma}{r_c} + \frac{1}{2}\, \rho\, g\, d \cos \alpha \qquad \text{B-7}$$

and at the evaporator

$$\overline{p_e} = p_v - \frac{\sigma}{r_e} + \frac{1}{2} \rho g d \cos \qquad \text{B-8}$$

Thus, the capillary pumping becomes

$$\Delta p_{cap} = \overline{p_c} - \overline{p_e} = \sigma \left(\frac{1}{r_e} - \frac{1}{r_c}\right) \qquad \text{B-9}$$

The two radii of curvature can be determined from equations B-2 and B-6. The minimum evaporator radius is (B-2)

$$r_e = \frac{w}{2} \qquad \text{B-10}$$

and the maximum condenser radius

$$r_c = \frac{\sigma}{\rho g d \cos \alpha} \qquad \text{B-11}$$

We therefore obtain for the capillary pumping capacity of the groove

$$\Delta p_{cap} = \frac{2\sigma}{w} - \rho g d \cos \alpha \qquad \text{B-12}$$

The first term in B-12 represents the pumping without gravity; the second term represents the reduction due to gravity.

The above analysis applies only for an orientation of the groove less than $\alpha = 90^{\circ}$, i.e., for the upper half of the grooves. Applying equation B-12 to the bottom grooves ($\alpha > 90^{\circ}$) would require a convex miniscus which is impossible for a wetting fluid. The performance of the entire heat pipe can be evaluated by analyzing each groove separately (different α's) and then adding the contributions of all grooves.

APPENDIX C

STABILITY OF BUBBLES IN A COMPOSITE WICK

The existence of vapor or gas bubbles within a composite wick has been observed frequently. In this appendix several mechanisms are studied which could account for their stability and their eventual collapse. The following cases are considered.

a. No non-condensing gas is present and the temperature is uniform everywhere.

Consider a bubble submerged in a liquid as shown in Figure C-1.

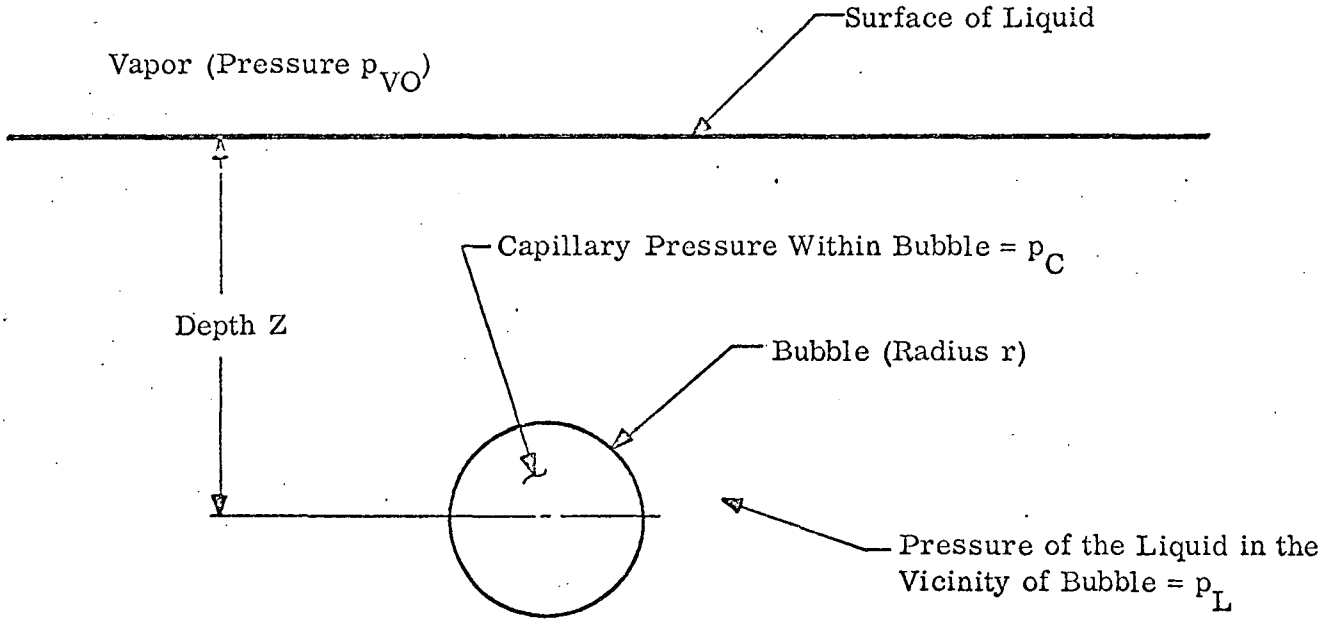

FIGURE C-1

SCHEMATIC OF BUBBLE

The pressure in the liquid in the vicinity of the bubble is

$$p_L = p_{VO} \pm \rho_L g z \qquad \text{C-1}$$

where ρ_L is the density of the liquid. The positive sign applies if the bubble is

submerged in a liquid below a free surface; the negative one applies if the bubble exists in a capillary above the free surface.

The capillary pressure within the bubble is determined by the surface tension

$$p_C = p_L + \frac{2\sigma}{r} \qquad \text{C-2}$$

The capillary pressure p_C is not necessarily equal to the pressure p_B within the bubble. In the absence of non-condensing gas the pressure in the bubble is given by:

$$p_B = p_{VO} \exp\left(\frac{-2\sigma}{r \rho_L RT}\right) \qquad \text{C-3}$$

Equation C-3 correlates the vapor pressure p_{VO} over a flat surface to that over a curved surface (Ref. C-1). The equilibrium vapor pressure in a bubble is lower than that over a flat surface at the same temperature.

Combining C-1 and C-2 we obtain for the capillary pressure within the bubble

$$p_C = p_{VO} \pm \rho_L g z + \frac{2\sigma}{r} \qquad \text{C-4}$$

The bubble will collapse or grow depending on whether the capillary pressure exceeds or is less than the pressure in the bubble, i.e.,

$$p_C \gtrless p_B \begin{cases} \text{collapse} \\ \text{stable} \\ \text{grow} \end{cases} \qquad \text{C-5}$$

Thus the requirement for a bubble to collapse is

$$p_{VO} \pm \rho_L g z + \frac{2\sigma}{r} > p_{VO} \exp\left(-\frac{2\sigma}{r \rho_L RT}\right) \qquad \text{C-6}$$

It can easily be shown that for the size of bubbles observed in a composite wick the exponential term on the right-hand side of C-6 is very close to unity. It will therefore be neglected in the following. Equation C-6 reduces to

$$\frac{2\sigma}{r} \pm \rho_L g z > 0 \qquad \text{C-7}$$

Ref. C-1: "Thermodynamics" by J. F. Lee and F. W. Sears, Second Edition, Addison-Wesley Publ. Co.

Equation C-7 states that all bubbles below a free liquid surface will always collapse (positive sign). Bubbles above a free surface (e.g. in a capillary) will only collapse as long as their radius does not exceed the static wicking height.

The rate of collapse can be estimated from the magnitude of the inequality in C-5. The difference between the two pressures give rise to a net rate of condensation. This rate is given by

$$G = \frac{p_C - p_B}{(2\pi RT)^{\frac{1}{2}}} \qquad \text{C-8}$$

where G is measured in grams/sec cm^2, R is the gas constant and T the absolute temperature.

Using this rate equation an estimate was made of the velocity with which long, "sausage" like bubbles within an artery should collapse. The rate was found to be 2×10^{0} cm/sec for bubbles within a .090" diameter artery and with methanol as the working fluid. Experimentally, a rate of 10^{-4} cm/sec was measured indicating that the above simple mechanism cannot account for the stability of bubbles.

Actually, the discrepancy between the model and the observed rate is not as drastic as the seven orders of magnitude seem to indicate. During condensation the latent heat is dissipated resulting in a temperature rise at the surface of the bubble. This temperature rise, in turn, results in an increase in vapor pressure thus slowing down the theoretical rate of collapse. Calculations showed, however that the slow-down is not sufficient to account for the extremely slow experimental rate.

b. No non-condensing gas is present, but a temperature non-uniformity exists within the system.

Assume that the temperature (T) in the vicinity of a bubble is slightly higher

---

Ref. C-2: "Kinetic Theory of Gases" by E. H. Kennard McGraw-Hill 1938

than in the rest of the system (T_O). According to equation C-5 the requirement for a stable bubble becomes

$$p_{VO}(T_O) + \frac{2\sigma}{r} = p_{VO}(T) \qquad \text{C-9}$$

(gravity effects and the small exponential term have been neglected). The required temperature gradient ($T - T_O$) can be estimated using the Clausius-Clapeyron relation

$$T - T_O = \frac{2\sigma}{r} \quad \frac{T}{h(\rho_V - \rho_L)} \qquad \text{C-10}$$

(h is the heat of evaporation, and ρ_L and ρ_V are the densities of liquid and vapor, respectively.) For a .090" diameter artery and with methanol as the fluid, the above temperature gradient was calculated to be .04°K. For ammonia the required temperature gradient is an order of magnitude smaller.

Hence, small temperature non-uniformities within the system could explain the observed stability of bubbles. In fact, existing bubbles can be made to grow or shrink in laboratory tests, depending on whether local heating or cooling is applied. However, the law of statistics rules out temperature gradients for being responsible for the observed stability of bubbles. Random temperature fluctuations should cause bubbles to grow or collapse with the same probability, in contrast to the experimentally observed long-term stability.

C. A small amount of non-condensing gas is present, but the temperature is uniform.

According to the preceding discussion a bubble is stable if the capillary pressure p_C is equal to the pressure within the bubble. In the presence of a non-condensing gas the pressure in the bubble is equal to the sum of the partial pressures of vapor π_V and gas π_G, i.e.,

$$p_B = \pi_V + \pi_G \qquad \text{C-11}$$

The partial pressure of the vapor is the same anywhere in the system and equal to the equilibrium vapor pressure p_{VO}. The capillary pressure p_C is still given by equation C-4, modified, however by an additional term which represents the partial pressure of the gas in the system.

$$p_C = p_{VO} + \frac{2\sigma}{r} + \pi_{GO} \qquad \text{C-12}$$

(Gravity has been neglected.) We therefore have the following requirement for a stable bubble

$$\cancel{p_{VO}} + \pi_G = \cancel{p_{VO}} + \frac{2\sigma}{r} + \pi_{GO} \qquad \text{C-13}$$

In a stable bubble the non-condensing gas is slightly compressed by the amount:

$$\Delta p = \pi_G - \pi_{GO} = \frac{2\sigma}{r} \qquad \text{C-14}$$

Numerically, this compression is small and, using the previous example, amounts to 0.3 mm Hg. A bubble, once it has been formed, will therefore collapse up to the point where sufficient compression has been achieved to satisfy the above equation. If the partial pressure of the gas within the system is of the same order of magnitude as the required compression the bubble will collapse approximately 50% until equilibrium is reached. After the bubble becomes stable the gas can escape only by dissolving in the liquid, a process which is inherently slow. The above process appears to be the only logical explanation for the observed stability of bubbles in composite wicks.

APPENDIX D

MATHEMATICAL MODEL OF THE INTERFACE BETWEEN THE VAPOR AND A NON-CONDENSING GAS IN A HEAT PIPE

In a heat pipe containing a non-condensing gas, in addition to the working fluid, separation of the two media occurs. The location of the interface is determined by the balance of pressures in the vapor region and within the non-condensing gas. The analysis presented here describes the axial variation of concentration of the two media in the vicinity of the interface. The temperature distribution along the wall is closely related to the concentration and is included in the analysis.

Schematically the distribution of concentration is illustrated in Figure D-1. On the vapor side, the concentration of vapor approaches 100% and that of the gas approaches zero. The converse is true on the gas side. In the vicinity of the interface both components are present at a finite concentration. The wall temperature is constant in the vapor region and decreases along the interface toward the (lower) gas temperature.

A mathematical model describing the variation of concentrations and temperature near the interface has been developed. It is based on the following simplifying assumptions:

(1) The vapor and the gas follow the ideal gas law.

(2) Only one-dimensional (axial) gradients are considered. There is no radial gradient of either concentration or temperature.

(3) The partial pressure of the vapor is uniquely determined by the equilibrium vapor pressure at the given wall temperature.

(4) Temperature gradients through wick and wall are neglected.

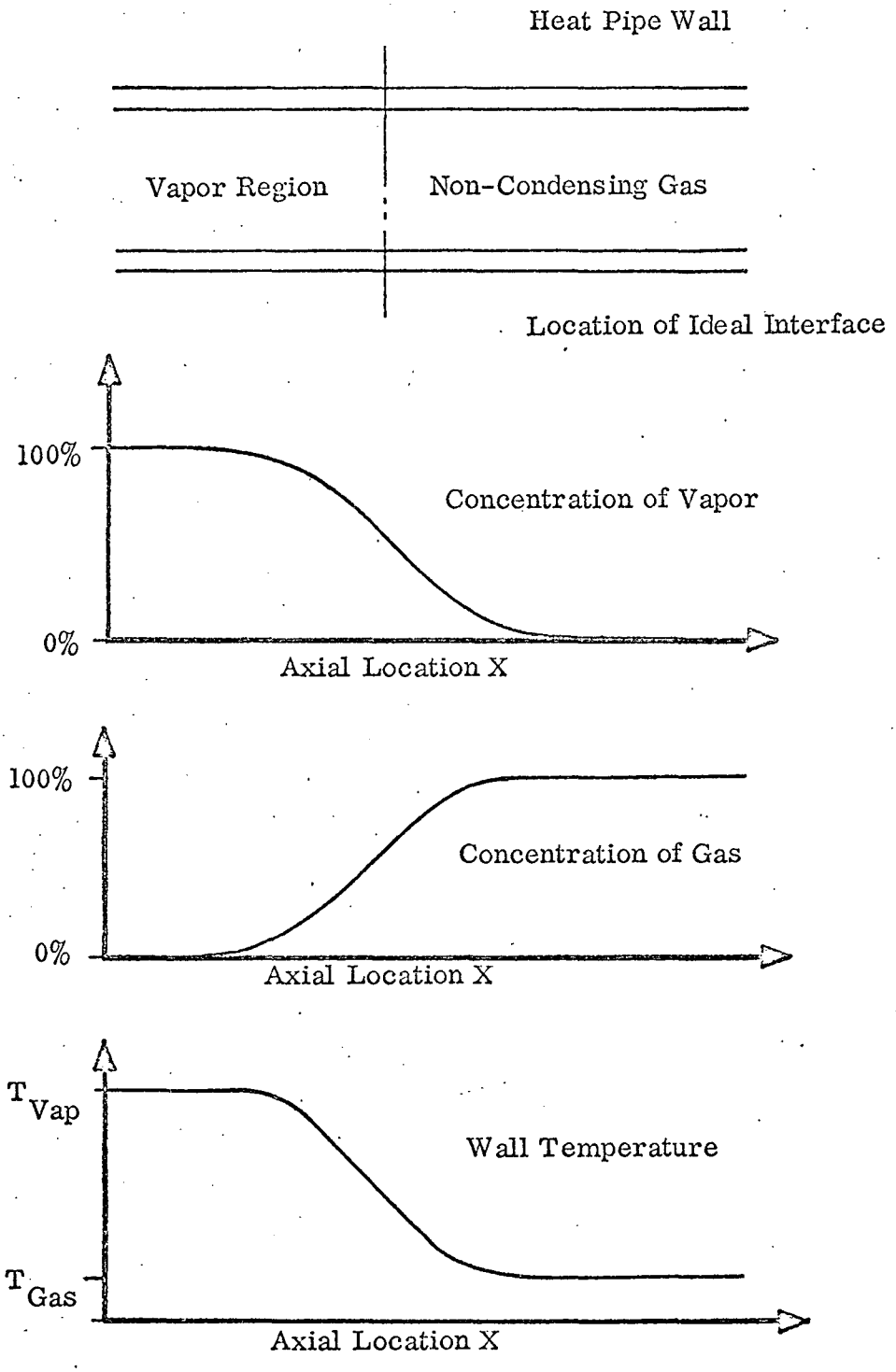

FIGURE D-1

SCHEMATIC OF THE DISTRIBUTION OF CONCENTRATION AND TEMPERATURE IN THE VICINITY OF THE INTERFACE

(5) Steady state exists.

(6) The geometry of the pipe (diameter, wall, wick, etc.) does not change in axial direction. The heat transfer coefficient for external heat removal from the pipe is also constant.

(7) The total pressure (sum of the partial pressures of vapor and gas) is constant along the pipe.

The following equations describe the gradients in the interface region.

The sum of the partial pressures of vapor and gas is constant everywhere and equal to the total pressure within the heat pipe:

$$p_v + p_g = p_o = \text{constant} \qquad \text{D-1}$$

(p_v = partial pressure of the vapor; p_g = partial pressure of the gas; p_o = total pressure in the heat pipe).

Both components, i.e., the vapor and the gas, follow the equation of state of an ideal gas:

$$p_v = n_v k T \qquad \text{D-2}$$

$$p_g = n_g k T \qquad \text{D-3}$$

(n_v and n_g are the particle densities of vapor and gas, respectively; k = Boltzmann Constant, and T is the common temperature of vapor and gas).

The equilibrium between vapor and gas is determined by the relative diffusion of vapor and gas. The diffusion equation for each component can be written as:

$$\frac{d N_v}{dt} = A n_v W - D_v A \frac{d n_v}{dX} \qquad \text{D-4}$$

$$\frac{d N_g}{dt} = A n_g W - D_g A \frac{d n_g}{dX} \qquad \text{D-5}$$

In the preceding equations, $\frac{d N_v}{dt}$ and $\frac{d N_g}{dt}$ are the particle fluxes per unit area and unit time (e.g., diffusing particles/cm^2 sec). The first terms on the righthand side of equations D-4 and D-5 represent the particle flows due to mass flow of the mixture (velocity W in cm/sec). The last terms represent the diffusion. D_v and D_g are the diffusion constants of both constituents, A the cross-sectional area of the heat pipe, and $\frac{d n_v}{dX}$ and $\frac{d n_g}{dX}$ the axial particle density gradients.

During steady state, there can be no net motion of the non-condensing gas, the particle flux of the gas must therefore be zero.

$$\frac{d N_g}{dt} = 0 \quad \text{for all axial location X} \qquad \text{D-6}$$

The partial pressure of the vapor is determined by the local temperature since we assumed that equilibrium exists at all points between vapor and liquid within the wick.

$$p_v = p_v(T) \qquad \text{D-7}$$

The rate of change of vapor flow in axial direction can be equated to the condensation rate on the wall.

$$\frac{d}{dX}\left(\frac{d N_v}{dt}\right) = R S \qquad \text{D-8}$$

R is the rate of particles condensing on the wall (measured, e.g., in cm^{-2} sec^{-1}), S is the circumference of the tube.

The condensation rate R is related to the internal heat flux q_i on the wall by

$$q_i = R \lambda \qquad \text{D-9}$$

where λ is the heat of condensation per molecule. λ is, of course, related to the conventional heat of condensation h through $h = \lambda \frac{n}{\rho}$, where ρ is the mass density

of the vapor and n the particle density.

Finally, we have to consider the heat flowing by conduction along the walls of the heat pipe. This heat flow Q is given by the familiar conduction equation, viz:

$$Q = -S \delta K \frac{dT}{dX} \qquad \text{D-10}$$

(S = circumference of heat pipe, δ = wall thickness, and K = thermal conductivity of wall material).

The heat balance for the wall is given by the following equation:

$$\frac{dQ}{dX} = q_i S - q_e S \qquad \text{D-11}$$

The first term in the last equation represents the rate of change of the heat flow by conduction. The second term is the heat gain by condensation from the vapor and the third one the heat loss to the environment. Typically, this heat loss term is represented by:

$$q_e = h (T - T_o) \qquad \text{D-12}$$

where h is the heat rejection coefficient and T_o the sink temperature. In the case of radiative heat rejection to the enviornment equation D-12 would be replaced by the appropriate equation for radiation.

The preceding 12 equations describe the stated problem completely. There are 12 unknows, viz:

p_v	p_g	T
n_v	n_g	W
N_v	N_g	R
		q_i
		q_e
		Q

Each one of these parameters is a function of X, the axial location on the heat pipe. The diffusion constants D_v and D_g are functions of the concentrations n_v and n_g, and, therefore, also vary along the heat pipe.

A solution of the set of equations can be obtained by numerical methods. The boundary conditions for both sides of the interface are well defined and the differential equations can be solved.

The numerical solution will yield the following information regarding the interface between a condensing and a non-condensing gas in a heat pipe:

(1) Temperature distribution along the wall.

(2) Concentration and partial pressures of both constituents within the heat pipe.

(3) The distribution of the rejected heat along the heat pipe.

Numerical solutions may easily be obtained with the help of standard computer routines. Such results would contribute greatly to the understanding of the behaviour of variable conductance heat pipes.

APPENDIX E

TESTING OF HEAT PIPE PROTOTYPES

After fabrication each heat pipe was vapor degreased with trichlorethane, flushed with methanol, evacuated and helium leak checked. Prior to charging with Freon 21, the pipes were outgassed at 220°F for 45 minutes under high vacuum.

The heat pipes were performance checked prior to delivery. The test set-up is shown in Figure E-1.

FIGURE E-1

TEST SETUP FOR PERFORMANCE CHECK

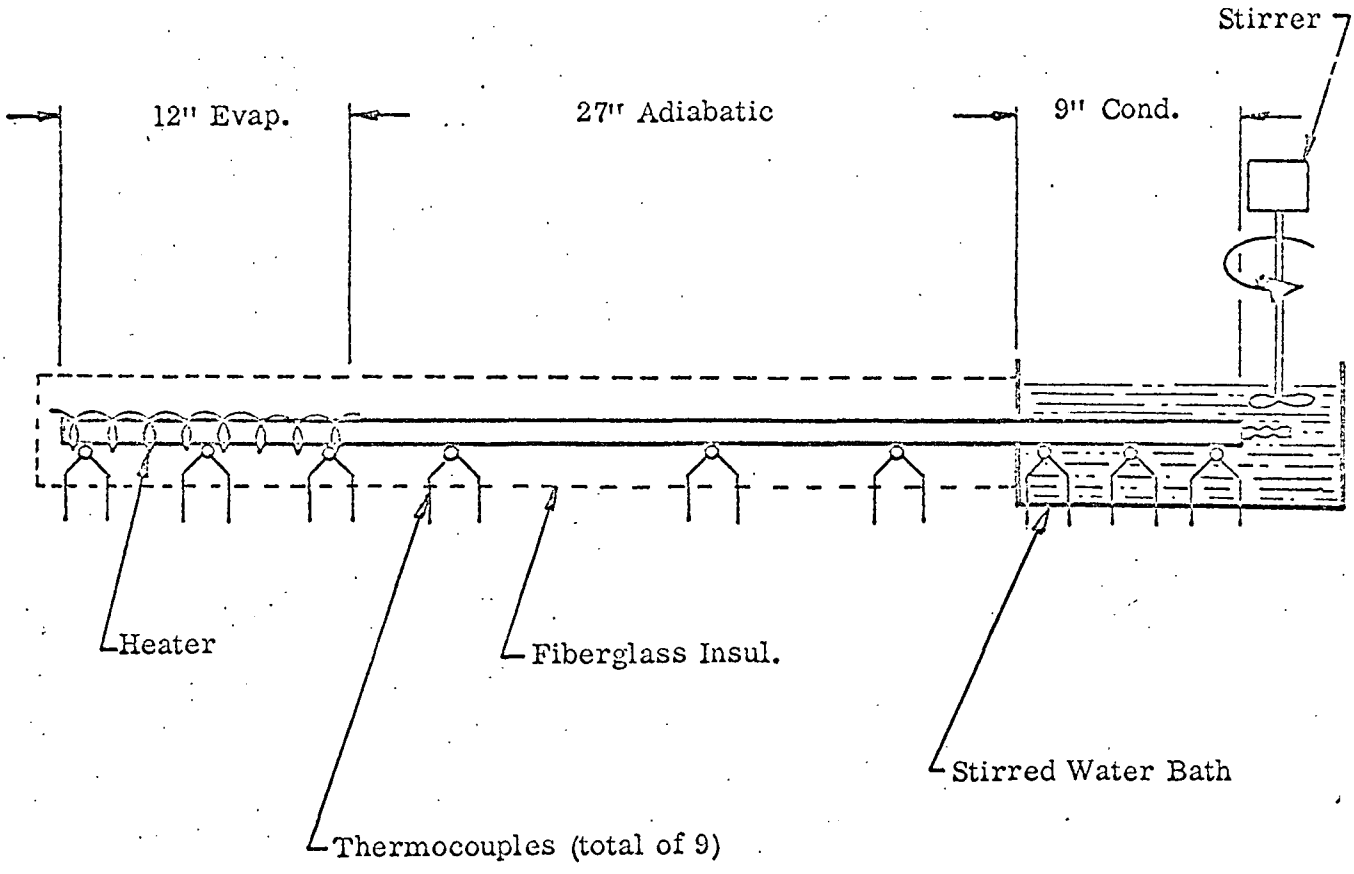

Leveling of the pipes was done by means of a Theodolite (Wild T2) with an accuracy of $\pm$ .005 inches. During the tests, the operating temperature (as measured on the adiabatic section) ranged from 17°C to 45°C. Since the temperature of the water bath was approximately constant at 10-15°C the vapor temperature was controlled by the condenser ΔT. This ΔT is a function of heat flow and of the wick geometry.